Channel II photocurrent quantification in narrow optical gap polymer-fullerene solar cells with complimentary acceptor absorption

Yuliang Zhang, Ajay K. Pandey' , Kristen Tandy, Gitish K. Dutta, Paul L. Burn, Paul Meredith, Ebinazar B. Namdas, and Satish Patil

Citation: Appl. Phys. Lett. **102**, 223302 (2013); doi: 10.1063/1.4808386
View online: http://dx.doi.org/10.1063/1.4808386
View Table of Contents: http://aip.scitation.org/toc/apl/102/22
Published by the American Institute of Physics

Channel II photocurrent quantification in narrow optical gap polymer-fullerene solar cells with complimentary acceptor absorption

Yuliang Zhang,[1] Ajay K. Pandey,[1,a)] Kristen Tandy,[1] Gitish K. Dutta,[2] Paul L. Burn,[1] Paul Meredith,[1] Ebinazar B. Namdas,[1] and Satish Patil[2]
[1]*Centre for Organic Photonics & Electronics, The University of Queensland, Brisbane QLD 4072, Australia*
[2]*Solid State and Structural Chemistry Unit, Indian Institute of Science, Bangalore 560012, India*

(Received 27 March 2013; accepted 17 May 2013; published online 6 June 2013)

Most charge generation studies on organic solar cells focus on the conventional mode of photocurrent generation derived from light absorption in the electron donor component (so called channel I). In contrast, relatively little attention has been paid to the alternate generation pathway: light absorption in the electron acceptor followed by photo-induced hole transfer (channel II). By using the narrow optical gap polymer poly(3,6-dithieno[3,2-b]thiophen-2-yl)-2,5-bis(2-octyldodecyl)-pyrrolo-[3,4-c]pyrrole-1,4-dione-5′,5″-diyl-*alt*-4,8-bis(dodecyloxy)benzo[1,2-b:4,5-b′]dithiophene-2,6-diyl with two complimentary fullerene absorbers; phenyl-C_{61}-butyric acid methyl ester, and phenyl-C_{71}-butyric acid methyl ester (70-PCBM), we have been able to quantify the photocurrent generated each of the mechanisms and find a significant fraction (>30%), which is derived in particular from 70-PCBM light absorption. © *2013 AIP Publishing LLC*.
[http://dx.doi.org/10.1063/1.4808386]

Donor-acceptor (D-A) bulk-heterojunction (BHJ) organic solar cells are attracting significant attention due to their potential for low cost solution processing onto large area flexible substrates at low temperatures. Improved light harvesting via the implementation of narrow optical gap polymers as electron donors has effectively doubled the efficiency of solution processed organic solar cells in the past 5 years to >8%.[1–6] In general, the primary photocurrent generation pathway (the so-called channel I pathway[7]) is considered to arise from photo-excitation of the donor followed by photo-induced electron transfer to the acceptor. This is particularly true for the most commonly used electron acceptor—the fullerene phenyl-C_{61}-butyric acid methyl ester (60-PCBM), which has a modest extinction coefficient in the solar harvesting window. However, the use of phenyl-C_{71}-butyric acid methyl ester (70-PCBM) as an acceptor has become increasingly popular.[8,9] 70-PCBM has significantly better absorption in the visible than 60-PCBM. Furthermore, non-fullerene electron acceptors are emerging with the potential to extend the D-A blend spectral range. As such, the concept of the channel II pathway, whereby photo-current is generated by direct absorption in the electron acceptor followed by photo-induced hole transfer to the electron donor, is an equally important route to generate free charges in complementary D-A blends.[7,10]

Exploiting and optimizing this strategy requires a detailed understanding of the relative photocurrent contributions and kinetics of charge generation via the two channels. As with virtually every aspect of organic solar cell science, the detailed kinetics and dynamics of carrier generation and extraction are system, architecture, and processing specific. In this letter, we address the broad question: how efficient is the free charge generation yield when photons are harvested by absorption by the fullerene versus the traditional route of photon harvesting through the polymeric electron donor? To this end, we have used the polymer donor poly(3,6-dithieno[3,2-b]thiophen-2-yl)-2,5-bis(2-octyldodecyl)-pyrrolo-[3,4-c]pyrrole-1,4-dione-5′,5″-diyl-*alt*-4,8-bis(dodecyloxy)benzo[1,2-b:4,5-b′]dithiophene-2,6-diyl (PTTDPP-BDT) that has distinct red absorption with a peak at 780 nm.[11] PTTDPP-BDT was blended with 60-PCBM and 70-PCBM, respectively, to fabricate single junction devices. By comparing the External Quantum Efficiencies (EQEs) achieved with each fullerene, we have been able to quantify the relative contributions and magnitudes of photocurrent generated via each of the channels, I and II, in these devices.

The molecular structures and film absorption spectra of pristine PTTDPP-BDT and the fullerenes are shown in Figures 1 and 2(a), respectively. The composite absorption spectra of PTTDPP-BDT with different fullerene blends (at blend ratio of 1:3; by wt.) are shown in Figure 2(b). As evident from Figure 2(a), the absorption spectra of PTTDPP-BDT, 60-PCBM, and 70-PCBM are complementary in nature. 60-PCBM and 70-PCBM are very similar acceptors in terms of their electronic properties,[8,9,12,13] charge mobility, and energetics.[14] Hence, to first order, the use of two spectrally different fullerene acceptors in conjunction with a mostly red absorbing polymer opens up the possibility of tracking the photocurrent generation back to the primary absorption events. The PTTDPP-BDT absorption is weak in the UV and green which is compensated for by 70-PCBM. On the other hand, 60-PCBM mostly absorbs in the UV, so only partially compensates the lack of polymer absorption in the green. We note that given the poor photoluminescence yield of the fullerenes, in general, the probability of energy transfer from 60- or 70-PCBM to the polymer would be insignificant. Thus, free carrier generation in the present combination of materials will proceed primarily through either the channel I and/or channel II mechanism. A typical architecture of our bulk-heterojunction cells is schematically presented in Figure 1.

Organic solar cells were prepared on pre-patterned indium-doped tin oxide (ITO) substrates supplied by Kintec,

a)Author to whom correspondence should be addressed. Electronic mail: a.pandey@uq.edu.au

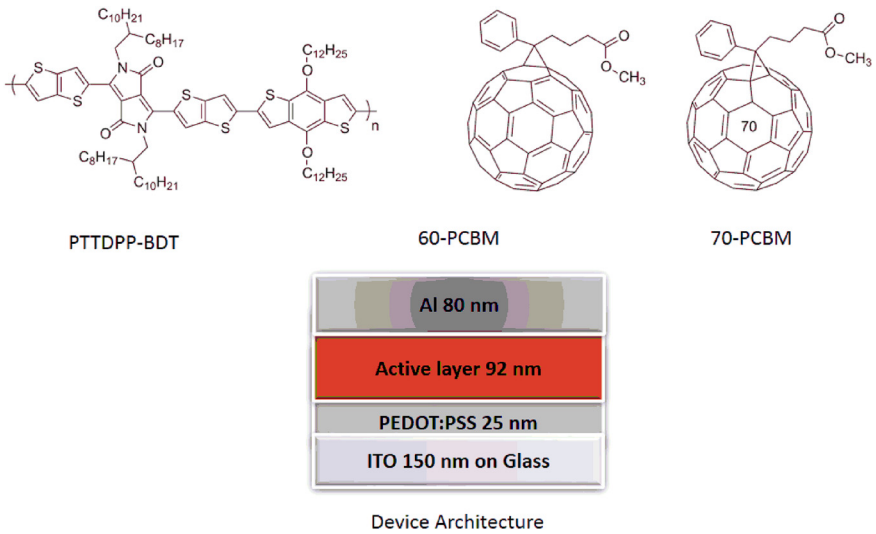

FIG. 1. The molecular structures of PTTDPP-BDT, 60-PCBM, 70-PCBM, and schematic architecture of the organic solar cell test devices.

Hong Kong. The substrates were first cleaned in warm detergent (Alconox), followed by sequential sonication in deionized water, acetone, and finally in 2-propanol for approximately 6 min each. The substrates were then blown dry with nitrogen. Poly(ethylenedioxythiophene):poly(styrenesulfonic acid) (PEDOT:PSS, Baytron P VP Al 4083) was spin-coated at 5000 RPM for 120 s and then baked on a hot plate for 20 min at 170 °C in air to give an ~25 nm thick layer. The final device fabrication steps were then carried out inside a nitrogen filled glove box with low oxygen and moisture content (<0.1 ppm). Stock solutions of polymer (7 mg/ml) and [70 or 60]-PCBM (7 mg to 28 mg/ml) were prepared in *o*-dichlorobenzene (DCB) and mixed in 1:1 ratios by volume in order to achieve blend ratios (by wt.) of 1:1, 1:2, 1:3, and 1:4. The active layers were fabricated by spin-coating the blend solutions onto the PEDOT:PSS layer at 1300 rpm for 30 s before being immediately placed in a covered Petri dish (~9 cm diameter) for slow drying (~5 min). The dry substrates were then baked at 60 °C for 20 min on a hotplate before metallization. The devices were completed by depositing the top electrode by thermal evaporation. Al (80 nm) was deposited under vacuum (1×10^{-6} mbar) at an initial rate of 0.4 A/s, which was then increased to 1.5 A/s to give an active device area of 0.2 cm^2. Each substrate contained 6 devices. The final architecture of the devices was glass/ITO/PEDOT:PSS/BHJ-active layer/Al.

Silicon wafers were used as substrates for the spectroscopic ellipsometry (SE). The SE measurements were performed with a J.A. Woollam VUV-VASE (GEN II) spectroscopic ellipsometer with autoretarder. J.A.Woollam WVASE32 software was used to fit the data. The wafers were first cleaned in an ultrasonic bath in acetone and 2-propanol for approximately 6 min each. The substrates were then blown dry with nitrogen. In order to get different film thicknesses, the BHJ samples were spin-coated onto the cleaned silicon wafers at spin speeds in the range of 1000 to

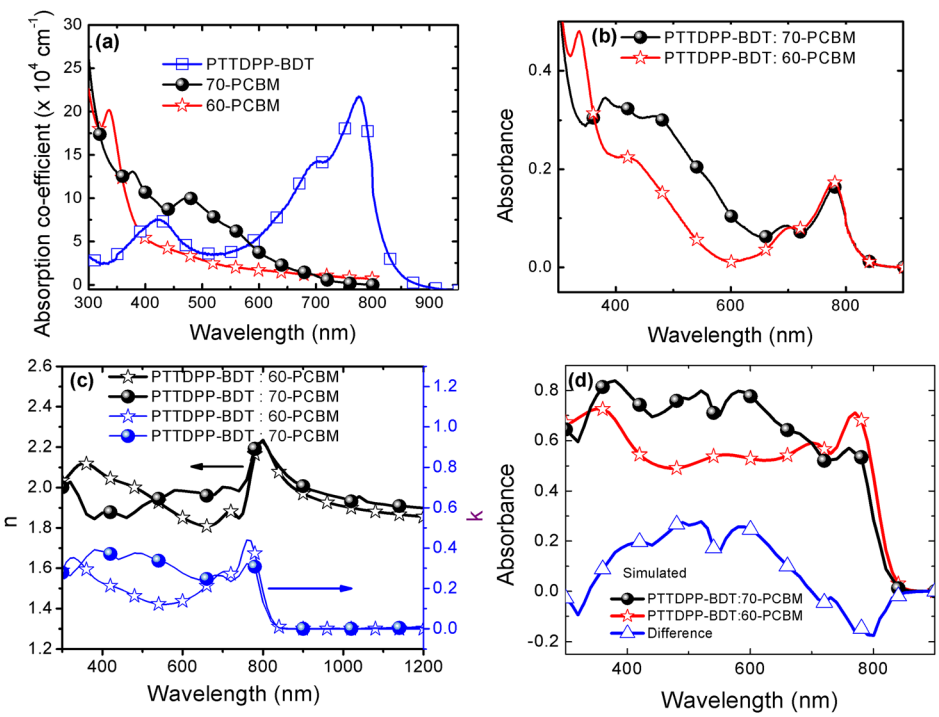

FIG. 2. (a) Absorption coefficients of the pristine materials measured in solid state, (b) composite optical absorption measured on glass substrates, (c) optical constants (n and k) of polymer-fullerene blends at the 1:3 ratio; and (d) composite optical absorption simulated using these optical constants in devices of PTTDPP-BDT:60-PCBM and PTTDPP-BDT:70-PCBM blends at a film thickness of 92 nm.

1500 rpm for 25 s. The SiO_2 layer thickness was modeled to be 2 nm.

One sun current density-voltage (*J-V*) data were acquired in an inert environment (<0.1 ppm of O_2 and H_2O) using a Keithley 2400 source measure unit in a 4-point source-sense configuration to eliminate the wire and contact resistances. The simulated Air Mass 1.5 Global (AM1.5G) irradiance was provided by an ABET Technology Sun 2000 Solar Simulator with irradiation intensity of 1000 W m^{-2} as determined by a National Renewable Energy Laboratory (NREL)-calibrated silicon reference cell. EQE measurements were made with a PV Measurements, Inc., QEX7 setup.

For optical spectroscopy, pristine PTTDPP-BDT, 70-PCBM, and 60-PCBM films were spin-coated onto quartz substrates. UV-visible absorption spectra were taken using a Cary 5000 UV-Vis spectrophotometer. The film thicknesses were measured using a Dektak 150 profiler.

In the first step of our study, we optimized the photoresponse of the polymer-fullerene blends by varying the blend ratio. Figure 3(a) shows the evolution of photocurrent at short-circuit (J_{sc}) as the amount of fullerene is varied. As with several narrow optical gap non-crystalline polymers, the photocurrent improves with increasing amounts of fullerene and reaches a maximum at a ratio of 1:3 (for both 60-PCBM and 70-PCBM) by weight. In line with general expectations, at all blend ratios, the photocurrent generated in the PTTBPP-BDT polymer with 60-PCBM is always lower than that with 70-PCBM. Once the optimum blend ratio was determined, we used a transfer matrix-based optical model to optimize the active layer thicknesses. This approach is useful since it simulates the overall device performance by predicting the photocurrent as a function of materials and architecture.[15,16] We used the transfer matrix model originally developed by van de Lagemaat at the NREL to estimate the electric field intensity (proxy for free carrier generation) produced from photon absorption as a function of wavelength and location within the active layer. The simulation is based on the model presented by Pettersson *et al.* and requires thickness (*d*), refractive index (*n*), and extinction coefficient (*k*) of each layer as input parameters.[17] The *n* and *k* of the active materials were determined from variable angle SE (VUV-VASE). Figure 2(c) shows the optical constants for optimized blends (at a ratio of 1:3) for PTTDPP-BDT:60-PCBM and PTTDPP-BDT:70-PCBM that were extracted from the ellipsometric data. Optical constants for other layers such as ITO, PEDOT:PSS, and Al were obtained from VASE by NREL and incorporated into the software as a database.

Figure 3(b) shows the simulated thickness dependent photocurrent for PTTBPP-BDT:60-PCBM and PTTBPP-BDT:70-PCBM. The simulation predicts a sharp increase in photocurrent up to a thickness of 90 nm, above that the increase is nominal. The model assumes that every photon absorbed gives rise to a free charge, that is, the internal quantum efficiency (IQE) is 100%. In this context, it is important to note that the short circuit current values are only relative—losses due to recombination and imperfect carrier extraction are not accounted for. These effects become increasingly pronounced in non-crystalline donor polymers at thicker active layers (>200 nm). Armed with knowledge of the best blend ratio and an approximate optimized thickness, one can then proceed with a reasonably tight experimental optimization scheme, the results of which are presented in Figures 3(c) and 3(d). The best devices consisted of a PTTBPP-BDT:70-PCBM active layer thickness of 90–95 nm and exhibited an average power conversion efficiency (PCE) of 3.1%, short circuit current (J_{sc}) of 9.4 mA cm^{-2}, open circuit voltage (V_{oc}) of 0.61 V, and fill factor (FF) of 0.54. From Figure 3(d), we see that the experimental results qualitatively agree with the simulated results, wherein

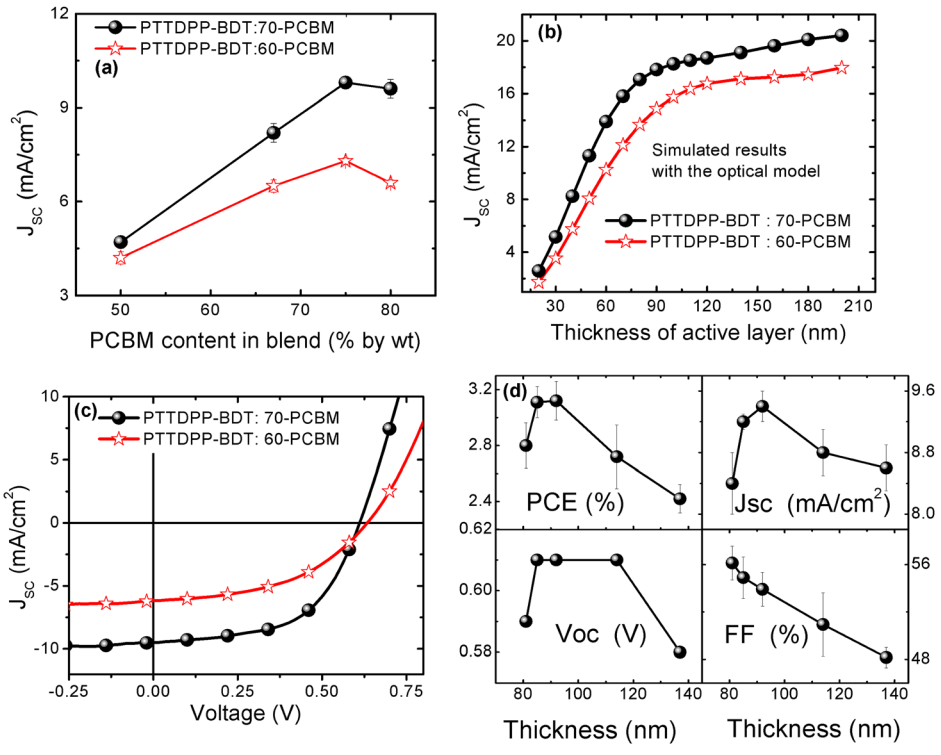

FIG. 3. (a) Optimization of the fullerene ratio in the blend with PTTDPP-BDT—short circuit current versus fullerene ratio (% content in blend by wt.); (b) active layer thickness optimization using a transfer matrix based optical simulation—short circuit current density versus active layer thickness; (c) typical J-V (current density–voltage) characteristics of two PTTDPP-BDT devices with 60-PCBM and 70-PCBM at an identical blend ratio (1:3) and thickness (92 nm); and (d) experimental active layer thickness optimization—photovoltaic parameters of PTTDPP-BDT:70-PCBM devices versus active layer thickness (noting 60-PCBM returned similar trends).

J_{sc} first rises up to an active layer thickness of 90 nm. The sharp fall in current above this thickness is likely due to the aforementioned effects (largely enhanced recombination losses) that are not accounted for in the simulations under the 100% IQE assumption. A similar optimization trend was observed for PTTDPP-BDT:60-PCBM devices (data not presented). It is important to note that multiple devices were fabricated and tested in each case, and the error bars in Figure 3(d) represent the standard deviation on the mean. Great care was taken to ensure appropriate white light calibration, and in general, the short circuit white light current agreed with the integrated EQE to be within 8%.

Figure 3(c) compares typical current density-voltage (J-V) characteristics of a PTTDPP-BDT polymer blend with 60-PCBM and 70-PCBM at an identical blend ratio (1:3) and thickness (92 nm). The maximum photocurrent recorded with 60-PCBM was 6.5 mA/cm^2 and with 70-PCBM 9.4 mA/cm^2. Both values are considerably lower than the modeled maximum photocurrents due to recombination and incomplete carrier extraction. Furthermore, and as indicated in Figure 2(a), the lower photocurrent with 60-PCBM is almost certainly due to its poorer visible absorption. This is confirmed in Figures 2(b) and 2(d) where we compare the measured (UV-visible spectra of the active layers on glass substrates) and simulated absorptions in the device structure. The simulated absorption within the device stack, as well as the absorption difference spectrum, suggests absorption at the polymer's peak varies slightly in the two blends, the 60-PCBM blend being slightly higher. This is replicated in the EQE response as shown in Figure 4(a) for two typical devices, with an active layer thickness of 92 nm. We believe the slight enhancement in the 60-PCBM is due to simple cavity interference effects. In Figure 4(a), we also show the difference spectrum for the EQEs which was calculated by absolute subtraction of PTTDPP-BDT:60-PCBM from PTTDPP-BDT:70-PCBM. Here, two notable details emerge: (i) a broad positive (+ve) EQE extends from 370 nm to 680 nm (more photocurrent from the 70-PCBM blend in this region); and (ii) two small negative (−ve) EQE regions located in the blue and red are also observed (more photocurrent from the 60-PCBM blend in these regions). The first −ve EQE peak at 330 nm occurs exactly in the spectral region where the 70-PCBM blend shows −ve absorption with respect to the 60-PCBM blend. Also, the peak positions in the +ve absorption region (stronger 70-PCBM absorption) appears to align well with the corresponding +ve EQE peaks and shoulders. These observations strongly suggest that photocurrent is being generated by direct absorption in the fullerene components and hence that channel II is active in this blend combination.

To probe this hypothesis further, in Figure 4(b), we compare the EQE difference spectrum with the blend absorption difference spectrum and also see strong qualitative agreement. The first −ve EQE peak at 330 nm occurs exactly in the spectral region where the 70-PCBM blend shows −ve absorption with respect to the 60-PCBM blend. Also, the peak positions in the +ve absorption region (stronger 70-PCBM absorption) appear to align well with the corresponding +ve EQE peaks and shoulders. Again, this comparison strongly suggests that absorption by the fullerenes generates the spectral EQE differences.

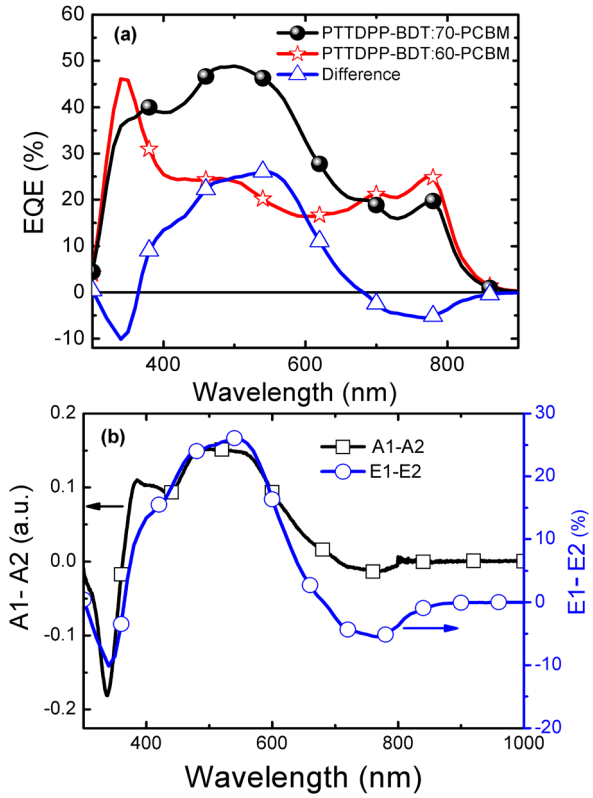

FIG. 4. (a) Comparative EQE spectra of PTTDPP-BDT:60-PCBM and PTTDPP-BDT:70-PCBM devices. The difference spectra are also shown, and are obtained by simple subtraction of the 60-PCBM consisting device response from the 70-PCBM device, and (b) comparison of the optical absorption (A1 and A2) and EQE difference spectra (E1 and E2) for 60-PCBM and 70-PCBM devices, where A1, A2 and E1, E2 represent absorption and EQE of photoactive layers composed of 70-PCBM and 60-PCBM, respectively. The two difference spectra are very similar showing good correspondence between the −ve and +ve regions, strongly suggesting absorption in the respective fullerenes generates the relative EQE differences.

Figure 4(a) can be used to approximate the relative contributions from the channel I and channel II processes in the 70-PCBM devices by integrating the photocurrents over the +ve EQE region, using following equation: $J = e \times \int_{\lambda 1}^{\lambda 2} PF(\lambda).EQE(\lambda)d\lambda$; where J is the photocurrent, e is the electron charge, $\lambda 1$ and $\lambda 2$ are 370 nm and 680 nm, respectively (the +ve EQE range), $PF(\lambda)$ is the spectral photon irradiance (AM1.5), and $EQE(\lambda)$ is the +ve external quantum efficiency from Figure 4(a). This calculation yields a photocurrent density generated by absorption in the 70-PCBM as high as 3.1 mA cm^{-2}, or 33% of the total. We note that the exact contribution from 70-PCBM phase would be more than 3.1 mA cm^{-2} in the devices as the calculations ignore the photon harvesting by 60-PCBM that exists in the wavelength range. By implication, the relative ratio of channel I to channel II photocurrent is ~70:30. Nevertheless, the results indicate that the majority of photons absorbed in the 70-PCBM are efficiently harvested.[18,19] Clearly, the judicious selection of an active layer composed of PTTDPP-BDT and commonly used fullerenes simplifies the complexity involved in elucidating photocurrent generation that would otherwise be a very complex task. The PTTDPP-BDT:fullerene system allows us to establish as well as quantify excitation pathways that lead to current generation.

Though the power conversion efficiency of this particular blend (3.1%) is moderate and far from meeting the requirements for commercial applications, the insights attained from this composition nonetheless clearly provide important understanding that would certainly be useful in designing the next generation of photoactive compounds for efficient organic solar cells.

To summarize, we have quantified the photocurrent in an organic solar cell generated via the channel II mechanism, that is by direct absorption of light by the electron acceptor, followed by photo-induced hole transfer to the electron donor. We achieved this using a narrow optical gap polymeric donor (PTTDPP-BDT) in combination with two commonly used fullerene-based acceptors (60-PCBM and 70-PCBM). The two fullerenes are electronically very similar but are spectrally different, and the use of the narrow optical gap of the donor has allowed us to isolate the relative photocurrent contributions using EQE difference spectra. In particular, the contribution to the short circuit current density by 70-PCBM absorption in a fully optimized bulk heterojunction device was found to be at least 3.1 mA cm^{-2}, which makes up $\sim$33% of the overall experimental photocurrent. The results presented here provide a better understanding of charge generation in narrow optical gap polymer-fullerene solar cells, and also demonstrate that channel II is an important and useful photocurrent creation pathway in complementary acceptor-donor junctions.

Y.Z. is funded by a University of Queensland Research Scholarship (UQRS) and University of Queensland International Research Tuition Award (UQIRTA). G.K.D. thanks UGC for a Senior Research Fellowship (SRF). E.B.N. is a recipient of an Australian Research Council Future Fellowship (FT110100216), P.M. and P.L.B. are UQ Vice Chancellor's Senior Research Fellows and the work was part funded by the Australian Solar Institute and Queensland Government through the National and International Research Alliances Program. We would also like to acknowledge the National Renewable Energy Laboratory (USA) for provision of the optical modeling software. This work was performed in part at the Australian National Fabrication Facility Queensland Node (ANFF-Q)—a company established under the National Collaborative Research Infrastructure Strategy to provide nano- and microfabrication facilities for Australia's researchers. Work in India was supported by the Department of Science and Technology (DST) through Project No. SR/S1/PC-40/2010.

[1]Z. He, C. Zhong, S. Su, M. Xu, H. Wu, and Y. Cao, Nat. Photonics **6**, 591 (2012).
[2]R. C. Coffin, J. Peet, J. Rogers, and G. C. Bazan, Nat. Chem. **1**, 657 (2009).
[3]Y. Y. Liang and L. P. Yu, Acc. Chem. Res. **43**, 1227 (2010).
[4]H. X. Zhou, L. Q. Yang, S. B. Liu, and W. You, Macromolecules **43**, 10390 (2010).
[5]P. L. T. Boudreault, A. Najari, and M. Leclerc, Chem. Mater. **23**, 456 (2011).
[6]Y. Y. Liang, Z. Xu, J. B. Xia, S. T. Tsai, Y. Wu, G. Li, C. Ray, and L. P. Yu, Adv. Mater. **22**, E135 (2010).
[7]Y. Fang, A. K. Pandey, A. M. Nardes, N. Kopidakis, P. L. Burn, and P. Meredith, Adv. Energy Mater. **3**, 54 (2013).
[8]J. M. Kroon, M. M. Wienk, W. J. H. Verhees, J. Knol, J. C. Hummelen, P. A. van Hal, and R. A. J. Janssen, Angew. Chem., Int. Ed. **42**, 3371 (2003).
[9]Y. Yao, C. J. Shi, G. Li, V. Shrotriya, Q. B. Pei, and Y. Yang, Appl. Phys. Lett. **89**, 153507 (2006).
[10]L. J. A. Koster, S. E. Shaheen, and J. C. Hummelen, Adv. Energy Mater. **2**, 1246 (2012).
[11]K. Tandy, G. K. Dutta, Y. Zhang, N. Venkatramaiah, M. Aljada, P. L. Burn, P. Meredith, E. B. Namdas, and S. Patil, Org. Electron. **13**, 1981 (2012).
[12]Y. Liang, Y. Wu, D. Feng, S.-T. Tsai, H.-J. Son, G. Li, and L. Yu, J. Am. Chem. Soc. **131**, 56 (2009).
[13]F. Huang, K. S. Chen, H. L. Yip, S. K. Hau, O. Acton, Y. Zhang, J. D. Luo, and A. K. Y. Jen, J. Am. Chem. Soc. **131**, 13886 (2009).
[14]S. Cho, J. H. Seo, K. Lee, and A. J. Heeger, Adv. Funct. Mater. **19**, 1459 (2009).
[15]A. Moliton and J. M. Nunzi, Polym. Int. **55**, 583 (2006).
[16]Q. L. Song and C. M. Li, Appl. Phys. Lett. **91**, 266103 (2007).
[17]L. A. A. Pettersson, L. S. Roman, and O. Inganäs, J. Appl. Phys. **86**, 487 (1999).
[18]N. C. Nicolaidis, B. S. Routley, J. L. Holdsworth, W. J. Belcher, X. J. Zhou, and P. C. Dastoor, J. Phys. Chem. C **115**, 7801 (2011).
[19]G. F. Burkhard, E. T. Hoke, S. R. Scully, and M. D. McGehee, Nano Lett. **9**, 4037 (2009).